Materials Science and Engineering C 68 (2016) 308–316

Contents lists available at ScienceDirect

Materials Science and Engineering C

journal homepage: www.elsevier.com/locate/msec

Water-dispersible triethylenetetramine-functionalized graphene: Preparation, characterization and application as an amperometric glucose sensor

Qunxiang Ren, Li Feng, Ronghua Fan, Xin Ge, Yingying Sun *

Department of Chemistry, Shenyang Medical College, Shenyang 110034, PR China

ARTICLE INFO

Article history:
Received 2 March 2016
Received in revised form 9 May 2016
Accepted 27 May 2016
Available online 01 June 2016

Keywords:
Functionalized graphene
Triethylenetetramine
Layer-by-layer covalent attachment
Glucose biosensors

ABSTRACT

The triethylenetetramine-functionalized graphene (TFGn) was prepared using graphene oxide (GO) and triethylenetetramine as raw materials through a one-step reaction under alkaline condition. The triethylenetetramine not only acted as cross-linker to combine GO, but also as reductant of GO. The TFGn was characterized by its ultraviolet spectrum (UV), Fourier transform infrared spectroscopy (FTIR), X-ray photoelectron spectroscopy (XPS), X-ray diffraction (XRD), Raman spectroscopy and Scanning electron microscopy (SEM). The results showed that triethylenetetramine was successfully grafted onto the surface of the GO through covalent bonding between amine and epoxy groups. The resultant TFGn was uniformly dispersed in water over several weeks, suggesting that the introduction of amino groups greatly increased the hydrophilicity of TFGn. The triethylenetetramine-functionalized graphene was then applied to fabricate glucose biosensors with IO_4^- oxidized glucose oxidase (GOx) through layer-by-layer (LBL) self-assembly by the covalent bonding between the aldehyde groups of GOx and amino groups of TFGn. The gold electrodes modified with the $(GOx/TFGn)_n$ multilayer films were studied by cyclic voltammetry (CV) and showed outstanding electrocatalytical response to the oxidation of glucose when ferrocenemethanol was used as an artificial redox mediator. The response increased with an increasing number of GOx/TFGn bilayers, indicating that the analytical performance, such as the sensitivity of the glucose biosensor, could be adjusted by tuning the number of deposited GOx/TFGn bilayers. The linear response range of the biosensor constructed with six bilayers of GOx/TFGn to the concentration of glucose can extend to at least 8 mM with a sensitivity of 19.9 μA mM^{-1} cm^{-2}. In addition, the sensor exhibited good stability due to the covalent interactions between the GOx and TFGn.

© 2016 Elsevier B.V. All rights reserved.

1. Introduction

Recently, a new two dimensional nanomaterial, denoted as graphene, has attracted considerable attention, and its applications are being widely explored. Graphene exhibits excellent electrical conductivity, strong mechanical strength, high thermal conductivity and a high surface area [1–6]. The planar morphology and larger surface area together with its excellent electrical conductivity make graphene an ideal material for electrochemical sensors [7–9], and graphene may perform better than any other carbon-based electrodes as a sensor material [10]. Recently it was shown that the graphene-based electrodes can provide excellent capability in ultra sensitive electrochemical detection of single nucleotide polymorphisms of DNA [11] and early detection of leukemia using DPV [12–13].

The graphene prepared by chemical reduction has a strong tendency to stack and easily form irreversible agglomerates through van der Waals interactions. As a result, graphene is poorly dispersible in most solvents, leading to the limited applicability of chemically reduced graphene. For biomedical applications, it is extremely important that prepared graphene is water-dispersible. This property is achievable by the appropriate surface functionalization of graphene through covalent and noncovalent methods [14–17]. The covalently-functionalized graphene is more stable compared with the noncovalently-modified graphene, which is functionalized through π-π interactions and van der Waals interactions.

Glucose oxidase (GOx) has been widely used in the construction of glucose sensors by virtue of its high selectivity for glucose and high activity over a broad range of pH values. Among various enzyme immobilization methods for the construction of glucose biosensors, the layer-by-layer technique through covalent and noncovalent approaches has intrinsic advantages for the assembly of ultrathin films due to the simplicity of the procedure and thickness controllability in the nanometer range [18]. The reports about graphene-based LBL film glucose sensors are very few in the literature [19–20]. Liu's group reported that the pyrene-functionalized GOx was utilized to fabricate enzyme electrodes

* Corresponding author.
E-mail addresses: syyxiluda@hotmail.com, chthrqx@hotmail.com (Y. Sun).

http://dx.doi.org/10.1016/j.msec.2016.05.124
0928-4931/© 2016 Elsevier B.V. All rights reserved.

by alternating layer-by-layer self-assembly of graphene and pyrene-functionalized GOx via noncovalent π-π stacking interactions. Gu and co-workers prepared a composite material $\{IL\text{-}RGO/S\text{-}RGO\}_n$ through the layer-by-layer method using amine-terminated ionic liquid (IL-NH_2) and sulfonic acid (SO^{3-})-functionalized graphene along with immobilized glucose oxidase on $\{IL\text{-}RGO/S\text{-}RGO\}_n$ films to fabricate a glucose sensor through electrostatic interaction. The driving force of the assembly processes of glucose oxidase described above is noncovalent interactions, which are not stable or strong enough, most certainly leading to their poor limited application. Meanwhile, in the work of Gu's group a monolayer of glucose oxidase was immobilized on a composite material, which affected the sensitivity of the sensor. To overcome these drawbacks, direct LBL enzymic covalent attachment for the fabrication of ordered multilayer films is believed to be more advantageous since they are robust enough to withstand elevated temperatures, attack by a polar solvent, mechanical abrasion, etc.

In this work, we demonstrate an effective method for preparing water-soluble triethylenetetramine-functionalized graphene, which was prepared using GO and triethylenetetramine as raw materials through a one-step reaction. The advantage of this preparation process is not using the EDC/NHS [21] as activator, and the hydrazine hydrate [16,22] as reductant. This avoids the aggregation of the triethylenetetramine-functionalized graphene under the complicated steps. The triethylenetetramine not only acted as cross-linker to combine GO, but also as reductant of GO. We attempt to apply the TFGn with many amino groups to construct glucose biosensors via the layer-by-layer covalent self-assembly method without any cross-linker. The amino groups of TFGn can react with the aldehyde groups of GOx through the formation of a Schiff base. Multilayer film electrodes were fabricated by alternating the deposition between TFGn and GOx until the desired number of bilayers was achieved. The electrochemical behaviors of the $Au/CA/(GOx/TFGn)_n$ electrode and its electrocatalysis activity for glucose were investigated. The resulting electrode exhibited outstanding bioelectrocatalytic response to the oxidation of glucose and very effective electrochemical communication between the successive layers. Furthermore, the covalent attachment technology overcame the stability drawback of multilayer films based on the layer-by-layer electrostatic adsorption technique. The TFGn involved cannot only immobilize GOx without the loss of biological activity but also enhance the measurement signal because of its fast electron-transfer and large working surface area.

2. Experimental

2.1. Reagents

Glucose oxidase (GOx, EC 1.1.3.4, from *Aspergillus niger*, 100 U mg^{-1}) was purchased from Amresco. Natural graphite flakes and triethylenetetramine came from the Sinopharm Chemical Reagent Co., Ltd. The cystamine dihydrochloride (CA) and ferrocene methanol were obtained from Aldrich. The other chemicals were of analytical grade. All of the solutions were prepared using doubly distilled water. Phosphate buffer solutions (PBS, 0.1 M, pH = 6.82) were employed as a supporting electrolyte. The glucose stock solutions were prepared with 0.1 M PBS and were allowed to sit overnight before use.

2.2. Apparatus

UV–vis absorption spectra were recorded on an Agilent Cary 300 spectrophotometer (Agilent Cary, Australia). The spectra were plotted in the wavelength range from 200 nm to 400 nm. Fourier transform infrared spectroscopy characterization of GO and TFGn was performed using a Perkin Elmer 2000 spectrophotometer (Perkin Elmer Inc., USA). The spectra were recorded using KBr pellets in the IR range of 4000–400 cm^{-1}. The surface composition and functional groups present in the GO and TFGn were determined using an X-ray photoelectron spectroscopy (XPS) system (Thermo VG ESCALAB250, USA). The scanning electron microscope (SEM) used in this work was a Hitachi TM-3000 SEM (Hitachi Limited, Tokyo, Japan). A X-ray diffraction (XRD) system (Rigaku Co., Tokyo, Japan) was used for the X-ray analysis with Cu Kα radiation (λ = 1.54051 Å). Step scanning was used with 2θ intervals from 6° to 60° and a residence time of 1 s. The Raman spectra of the GO and TFGn were carried out using the DXR smart Raman spectrometer (Thermo Fisher, USA) under the 532 nm laser excitation.

The cyclic voltammetric and amperometric measurements were performed on a CHI 760E electrochemical workstation (Shanghai Chenhua, China). Experiments were performed in a standard three-electrode cell (10 mL) with a modified Au as the working electrode, a saturated calomel electrode (SCE) as the reference electrode, and a platinum wire as the auxiliary electrode. The amperometric experiments of the $Au/CA/(GOx/TFGn)_n$ electrode with the sequential addition of a desired amount of glucose were carried out in a gently stirred air-saturated 0.1 M PBS buffer solution. The electrochemical impedance spectroscopy (EIS) measurements were performed in the presence of 5.0 mM $K_3[Fe(CN)_6]/K_4[Fe(CN)_6]$ (1:1) mixture as a redox probe in the frequency range between 0.1 and 100,000 Hz. All experiments were performed at room temperature.

2.3. Preparation of GO and TFGn

The GO was prepared by a modified Hummers method using expanded graphite as the precursor [23]. The GO (20 mg) was dispersed in doubly distilled water (20 mL) and sonicated for 1 h to homogeneously disperse the GO sheets in solution. Two milliliters of 1% NaOH and 20 μL of triethylenetetramine were sequentially added dropwise to the above-mentioned solution, and the reaction mixture was refluxed and stirred at 60 °C for 24 h. Then, the mixture was centrifuged and washed with doubly distilled water three times. The preparation process is shown in Scheme 1A.

2.4. Synthesis of aldehyde glucose oxidase

The aldehyde glucose oxidase was prepared by the methodology already demonstrated by Zaborsky [24] with slight modifications. A 74.4 mg sample of GOx was dissolved in 10 mL of phosphate buffer solution (0.1 M, pH = 6.8) and was reacted with 120 mg of sodium metaperiodate at 0 °C in the dark for 1 h. Then, 31 μL of ethylene glycol was added to the above solution, and the reaction was continued at room temperature for 30 min. The product was purified and concentrated with ultrafiltration (molecular weight cutoff of 30,000).

2.5. Fabrication of the $Au/CA/(GOx/TFGn)_n$ electrode

The gold electrode was polished to a mirror-like surface with 1.0, 0.3, and 0.05 μm alumina powder sequentially and then washed with water and ethanol for a few minutes in an ultrasonic bath, respectively. The electrode was dried with nitrogen steam for the next decoration. The clean electrode was immersed into an aqueous cystamine solution (20 mg/mL) in darkness for 2 h. After thiol adsorption, multilayer films of GOx/TFGn were fabricated by alternatively dipping the modified electrode into the GOx solution and the above TFGn solution each for 1 h. After each dipping step, the electrode was carefully washed with doubly distilled water and then dried with nitrogen. This process was repeated until the desired GOx/TFGn bilayer number was achieved. The modified electrode was denoted as $Au/CA/(GOx/TFGn)_n$. The assembly process is shown in Scheme 1B. In comparative experiments, the multilayer film was fabricated following the same process using a GO solution instead of a TFGn solution. The resulting electrode was abbreviated to $Au/CA/(GOx/GO)_n$. The $Au/CA/(GOx/GO)_n$ electrode was stored at 4 °C when not in use.

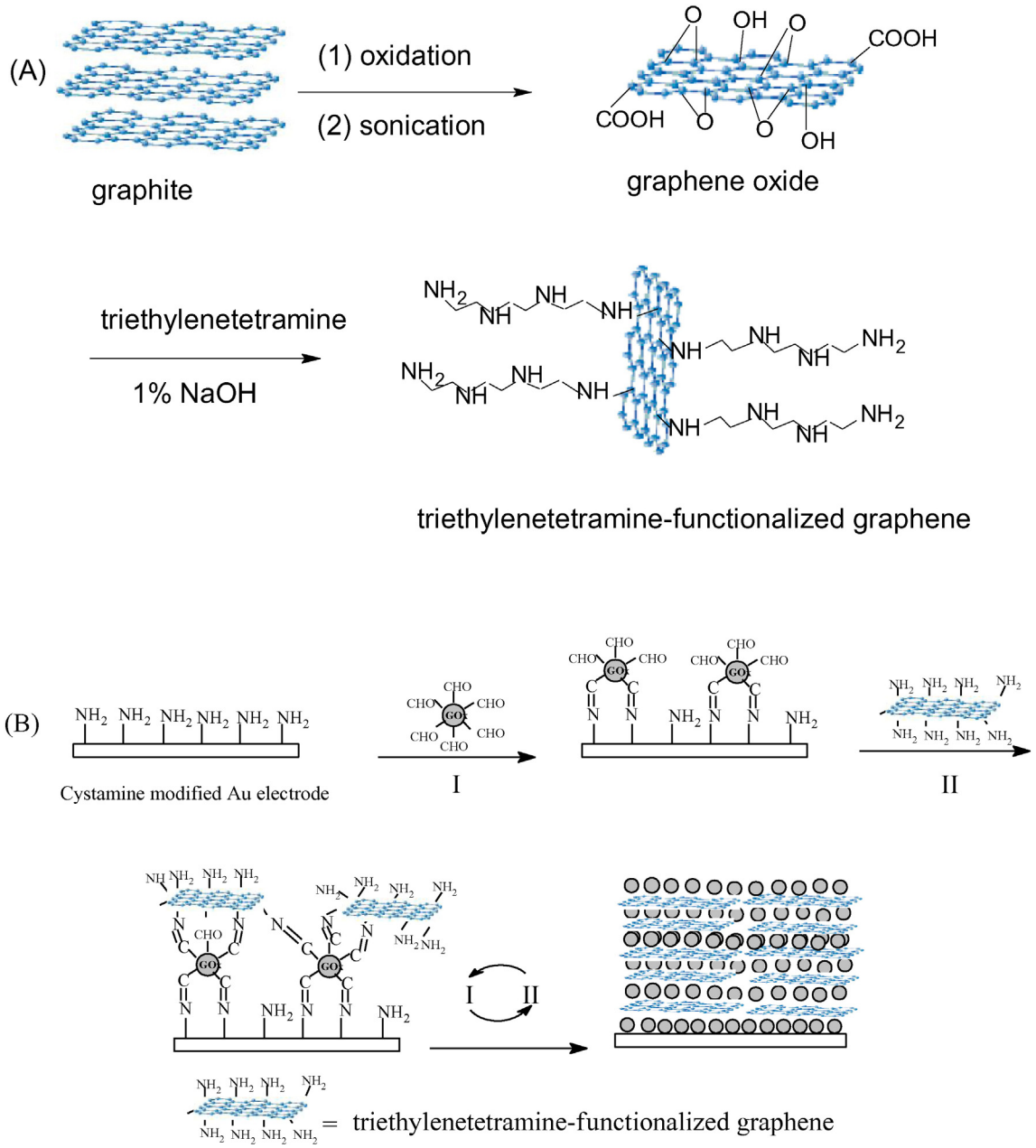

Scheme 1. (A) Preparation process of triethylenetetramine-functionalized graphene. (B) Stepwise assembly of the Au/CA/(GOx/TFGn)$_6$.

3. Results and discussion

3.1. Characterization of GO and TFGn

Fig. 1(A) shows the UV–vis absorption spectra of prepared graphene oxide and triethylenetetramine-functionalized graphene dispersed in doubly distilled water by means of an ultrasonication bath (1 h). The UV–vis spectrum of graphene oxide exhibited the following two characteristic features that can be used as a means of identification: a maximum at 231 nm, corresponding to the π → π* transitions of aromatic C—C bonds, and a shoulder at 300 nm, which can be attributed to n → π* transitions of C═O bonds [25]. In TFGn, the absorption band of the aromatic C—C bonds at 230 nm shifted to 257 nm indicating the restoration of a π-conjugated network. The shoulder peak of GO at 300 nm disappeared, most likely due to a decrease in the concentration of carboxyl groups [26].

The FT-IR spectra of different samples were recorded (as shown in Fig. 1(B)). The characteristic features related to GO were observed at 3367 cm^{-1} (O—H stretching vibrations), 1731 cm^{-1} (C═O stretching vibrations from carbonyl and carboxylic groups), 1621 cm^{-1} (C═C stretching vibrations of aromatic rings) [27], 1222 cm^{-1} (C—O stretching vibrations) [28], 1051 cm^{-1} (symmetric C—O—C stretching vibrations) and 853 cm^{-1} (asymmetric C—O—C stretching vibrations). The FT-IR spectrum of TFGn exhibited additional peaks due to N—H stretching vibrations at 3400 cm^{-1}, N—H bending vibrations at 1582 cm^{-1} [29] and the peak due to C—N stretching vibrations at 1357 cm^{-1}. The absorption peaks at 1731 cm^{-1} (C═O stretching), 1051 cm^{-1} (symmetric C—O—C stretching), and 853 cm^{-1} (asymmetric C—O—C stretching) disappeared. The FT-IR results not only demonstrated that the triethylenetetramine was successfully grafted onto GO, and the grafting reaction occurred between the amine groups of triethylenetetramine and the epoxy groups on the GO surface, but also confirmed that GO was reduced.

The GO and TFGn were characterized by XPS (Fig. 2). The full scan result of the GO showed two strong peaks at 284 and 532 eV, which were corroborated to C1s and O1s peaks. The grafting of triethylenetetramine

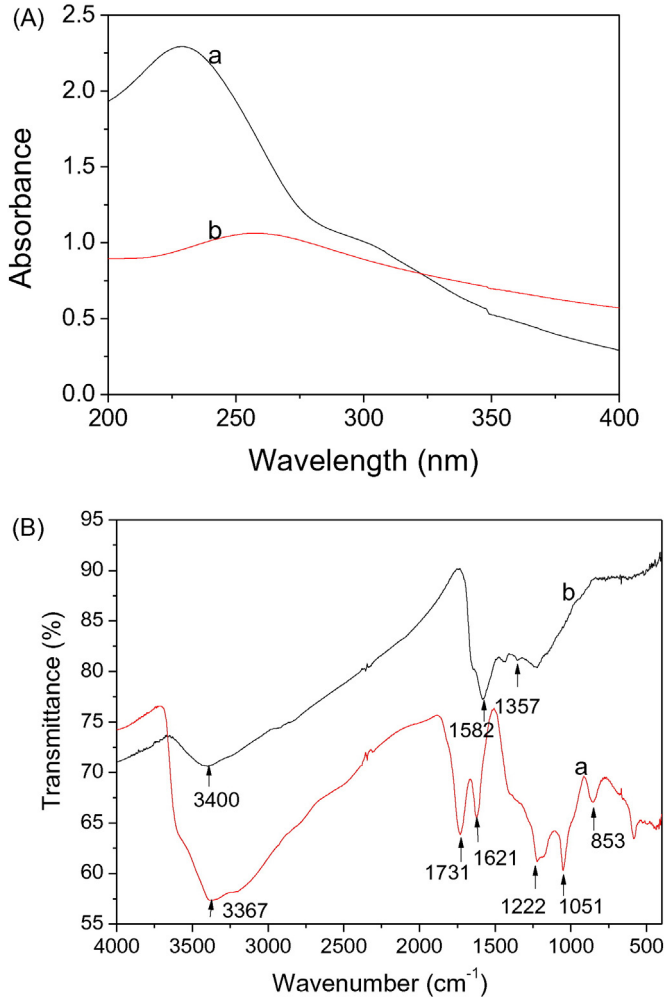

Fig. 1. UV–vis absorption spectra (A) and FTIR spectra (B) of prepared graphene oxide (GO) and triethylenetetramine-functionalized graphene (TFGn). (a) GO, (b) TFGn.

onto the GO surface resulted in an increase in the peak intensity of the C1s peak (284 eV) with a decrease in the O1s peak (532 eV). The peak intensity ratio of C1s/O1s greatly increased up to 1.83 (TFGn) from 0.58 (GO), indicating that most of the oxygen functional groups were removed. This result further confirmed that the graphene oxide was reduced. Moreover, the XPS spectrum of the TFGn showed a new peak at a binding energy of approximately 399 eV, which could be assigned to N1s, indicating the reaction between triethylenetetramine and GO.

To better study the effect of the triethylenetetramine on the deoxygenation of the GO, the C(1s) peaks of the GO and TFGn was deconvoluted (Fig. 2(C, D)). In the peak deconvolution, the peak centered at 284.5 eV was attributed to the C—C and C═C bonds. Other deconvoluted peaks located at the binding energies of 286.6, 287.8 and 289.0 eV were assigned to the C—O, C═O, and O═C—OH oxygen-containing functional groups, respectively [30]. From Fig. 2(C, D) it appears that the peak area ratios of the C—O, C═O and O═C—OH peaks to the C(1S) for the TFGn significantly decrease compared to that for the GO. The result means that most of the oxygen-containing functional groups of the GO were removed after the triethylenetetramine functionalization. Another peak component at 285.6 eV was assigned to the C—N bonds. In fact, the survey XPS spectrum of the GO reduced by the triethylenetetramine (Fig. 2(B)) confirmed presence of nitrogen in the TFGn. To further confirm the formation of the C—N bonds in the TFGn, the high resolution N(1s) peak was also deconvoluted, as shown in Fig. 2(E). In the peak deconvolution, the peaks centered at 400.9 and 399.1 eV were assigned to N–sp^2C and N–sp^3C [31–32], respectively. For triethylenetetramine functionalized graphene, the N–sp^2C peak is due to nitrogen incorporated in the graphitic structure of the sheets and the N–sp^3C peak can be assigned to existence of nitrogen in the triethylenetetramine and formation of the C—N bonds between the triethylenetetramine and the reduced GO sheets [31]. The high resolution N(1s) peak for the TFGn indicates the formation of C—N bonds in the TFGn, this conclusion is consistent with the results obtained based on the deconvolution of the C(1s) peak.

Changes in the chemical structure due to the grafting of triethylenetetramine were investigated using X-ray diffraction characterization, and the results are included in Fig. 3(A). The XRD pattern of GO shows a very intense narrow peak at approximately 10.8°, which is attributable to the (001) diffraction plane of GO [33], and a weak broad peak at approximately 22°, which is attributable to the (002) diffraction plane of the graphite. The presence of the (002) diffraction plane indicates that the GO partly reserved structure of the original graphite. Following modification with triethylenetetramine, the (001) diffraction peak of TFGn shifted to a smaller angle region (9.5°) and had a very weak intensity compared to that of GO, indicating that the triethylenetetramine was inserted into the GO sheets to increase the interlayer distances and most of the oxygen functional groups were removed.

Raman spectroscopy is a widely used and powerful technique for the characterization of graphene products [34–37]. The TFGn was further characterized by Raman spectroscopy, as shown in Fig. 3(B). The peaks located at 1346 cm^{-1} and 1586 cm^{-1} correspond to the D peak and G peak. The D band caused by a breathing mode of k-point phonons of A_{1g} symmetry of the defects involved in the sp^3-hybridized carbon bonds, and the G band originated from the first-order scattering of the E_{2g} phonons of the sp^2-hybridized carbon atoms [38]. The intensity ratio of the D band to the G band (I_D/I_G) is a measure of disorder degree. The intensity ratio I_D/I_G for the TFGn (1.1) is larger than that for the GO (0.9), indicating the generation of localized sp^3 defects within the sp^2 carbon network upon triethylenetetramine modification of the GO. In addition, the Raman spectrum of the TFGn displays a shoulder D + G band at 2916 cm^{-1} and a 2D band at 2683 cm^{-1}. The former is related to the defect of graphene and the latter is much sensitive to stacking of graphene sheets. For single-layer graphene sheets, the 2D band generally appears as a Lorentzian peak centered at 2679 cm^{-1}, while for multilayer graphene sheets (including 2–4 layers) the 2D band shows a wider peak with 19 cm^{-1} shift to higher wavenumbers [31]. In this work, the 2D peaks of the as-prepared GO and TFGn centered about 2690 cm^{-1} and 2683 cm^{-1}, respectively. The wavenumber position of the 2D peak for the TFGn is lower than that for the GO, indicating that the triethylenetetramine was inserted into the GO sheets to increase the interlayer distances.

Sample dispersion in water was studied. GO and TFGn dispersions (1.0 mg/mL) were sonicated for 10 min and allowed to settle for a week. Fig. 4(a) shows photographs of the dispersions of prepared graphene oxide and triethylenetetramine-functionalized graphene in doubly distilled water. The results showed that the prepared samples exhibited good dispersion properties in water. SEM was used to observe the dispersion. GO and TFGn dispersions were sonicated for 10 min and dropped onto silicon wafers. Fig. 4(b, c) shows SEM images of the GO and TFGn after drying. As shown in this figure, the GO and TFGn exhibited wrinkled graphene sheets. The appearance of GO and TFGn revealed the fact that the resulting samples were uniformly dispersed in water and exhibited no aggregation.

3.2. LBL covalent assembly of the Au/CA/$(GOx/TFGn)_n$ electrode

Here the LBL covalent self-assembly method was used to construct Au/CA/$(GOx/TFGn)_n$ multilayer film sensors. The assembly process is shown in Scheme 1B. First, the cystamine was immobilized onto the gold electrode surface through the formation of covalent S—Au bonds

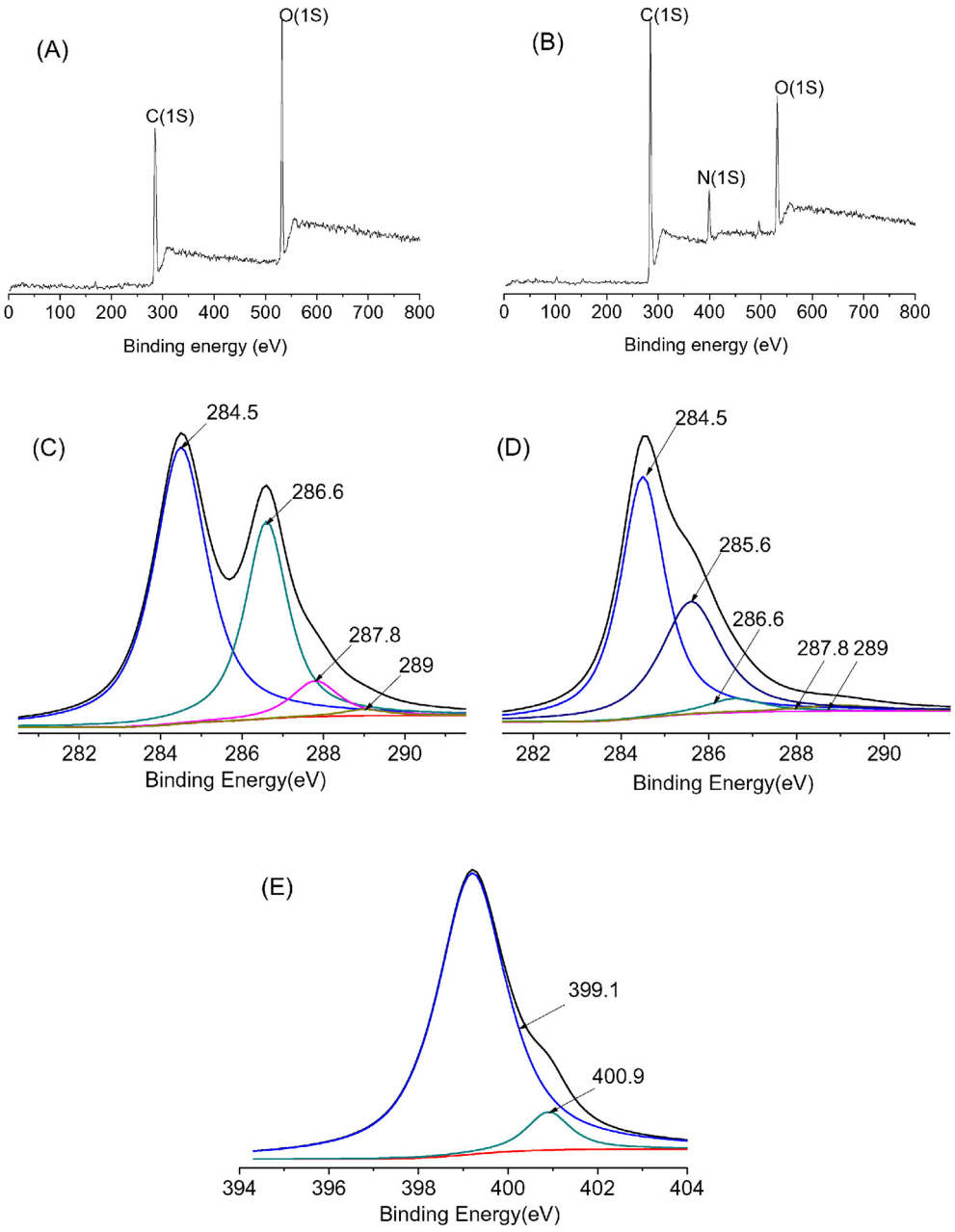

Fig. 2. XPS spectra: (A) The survey XPS spectrum of GO. (B) The survey XPS spectrum of TFGn. (C) The high resolution XPS of C(1S) of GO. (D) The high resolution XPS of C(1S) of TFGn. (E) The high resolution XPS of N(1S) of TFGn.

and provided a batch of amino groups directed towards the solution. Second, the amino groups of cystamine were allowed to react with the aldehyde groups of GOx molecules through the formation of a Schiff base. Then, TFGn molecules were covalently attached to GOx in the same manner. The successive repetition of the deposition of GOx and TFGn generated homogeneous and stable multilayer films with the desired number of bilayers. Different from other literature, in which the graphene and enzymes were generally cast or pasted onto the electrode surface [28,39–41], a feature of this assembly process is the formation of a covalent bond between the amino groups of cystamine and TFGn and the aldehyde groups of GOx.

3.3. Electrochemical impedance spectroscopy of the TFGn/GOx multilayer films

The assembly process of TFGn/GOx multilayer films on the Au electrode was confirmed by EIS, which is an effective method for probing the features of surface modified electrodes [42]. The Nyquist plot of the impedance spectrum includes a semicircle portion at high frequency and a linear portion at low frequency. The former corresponds to the charge transfer limited process and the latter corresponds to the diffusion process. The electron transfer resistance (R_{ct}) at the electrode surface is equal to the semicircle diameter, which can be used to describe the interface properties of the electrodes. Fig. 5 shows the impedance spectra represented as Nyquist plots (Z″ versus Z′) of electrodes modified with different numbers of TFGn/GOx in the presence of equimolar $K_3[Fe(CN)_6]/K_4[Fe(CN)_6]$. It can be seen from Fig. 5 that the bare gold electrode exhibited an almost straight line (Fig. 5(a)), which is characteristic of a diffusion limited electrochemical process. Assembly of GOx on the aminated electrode generated an insulating layer on the electrode surface that functioned as a barrier to the interfacial electron transfer. When the electrode was further modified by another insulating layer, TFGn/GOx, some significant differences were observed. This was shown by the increasing of Rct (Fig. 5(b–g)), and the charge

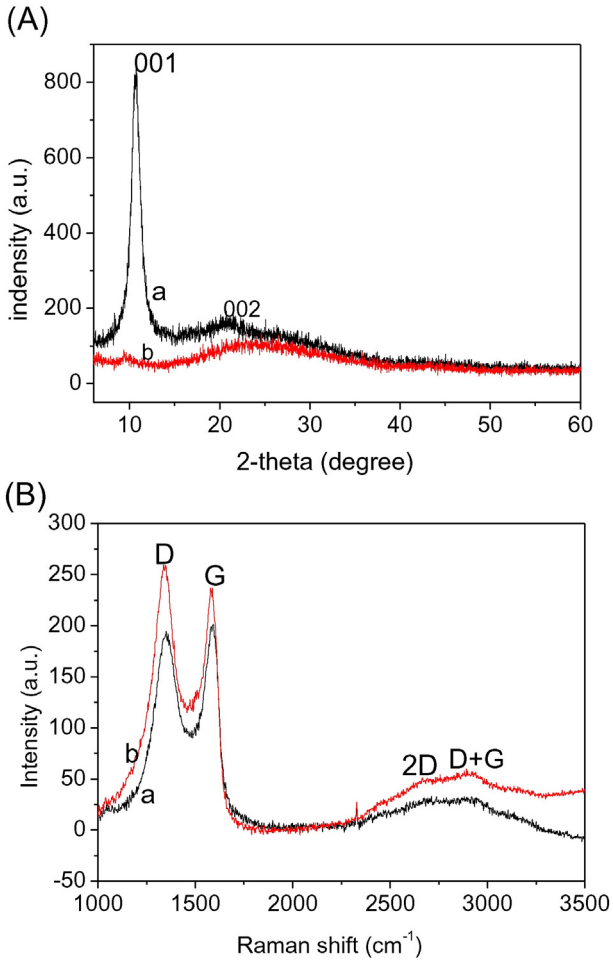

Fig. 3. The XRD spectra (A) and Raman spectra (B) of GO (a) and TFGn (b).

transfer resistances (R_{ct}) increased proportionately with an increasing number of attached bilayers, as shown in inset of Fig. 5. These results indicate that TFGn/GOx multilayer films have been immobilized onto the electrode in a uniform manner.

3.4. Electrochemical behavior of the Au/CA/(GOx/TFGn)$_n$ electrodes

Fig. 6 shows the cyclic voltammograms of an Au/CA/(GOx/TFGn)$_6$ multilayer film electrode in a 0.1 mol/L PBS solution with a pH of 6.8 containing 0.25 mmol/L ferrocenemethanol at different scan rates. As shown in Fig. 6, with an increasing scan rate, the CV peak currents of the Au/CA/(GOx/TFGn)$_6$-modified electrode increased in the scan rate range of 10–130 mV/s. The anodic and cathodic peak currents increased linearly with the square root of the scan rate (inset of Fig. 6), indicating that the electrochemical reaction of the (GOx/TFGn)$_6$-modified electrode was a diffusion controlled process.

3.5. Electrocatalytic oxidation of glucose at the Au/CA/(GOx/TFGn)$_n$ electrodes

Fig. 7 shows the cyclic voltammetric responses obtained from the Au electrodes modified with different numbers of GOx/TFGn bilayers in the presence of 20 mM glucose and 0.25 mM ferrocenemethanol. At a bare Au electrode, a pair of well-reversible redox waves with a peak potential separation of 0.06 V was observed, which was characteristic of the one-electron reversible redox reaction of Fc^+/Fc. When a significant amount of active enzyme was covalently assembled on the electrodes, the anodic current elevated with an increase in the number of GOx/TFGn bilayers at the same glucose concentration, and the cathodic current decreased (Fig. 7). When the number of GOx/TFGn bilayers reached 4, the cathodic current completely disappeared. This result suggested that the GOx had been successfully assembled onto the electrode surface and that the assembled GOx remained active. The electrocatalytic oxidation mechanism of glucose can be described by Eqs. (1)–(3) when ferrocenemethanol was used as an artificial redox mediator [43].

$$Fc \rightleftharpoons Fc^+ + e \quad (1)$$

$$GOx(FAD) + G \underset{k_{-1}}{\overset{k_1}{\rightleftharpoons}} GOx(FAD\text{-}G) \xrightarrow{k_2} GOx(FADH_2) + GL$$

$$GOx(FADH_2) + 2Fc^+ \xrightarrow{k_3} GOx(FAD) + 2Fc$$

In a comparative experiment, GO is used to construct a multilayer film sensor instead of TFGn. The electrocatalytic current of the resulting modified electrode did not show any improvement with an increasing number of bilayers because covalent bonds between the GOx and GO could not form.

In the absence of mass transport limitations, the surface coverage of active enzyme, Γ_{ET}, can be derived from ferrocenemethanol-mediated cyclic voltammograms using kinetic models reported in the literature [43–44], and plateau current I_p is expected to obey the following equation:

$$\frac{1}{I_p} = \frac{1}{2FS\Gamma_{ET}}\left(\frac{1}{k_3[Fc]} + \frac{1}{k2} + \frac{1}{k_{red}[G]}\right)$$

Here F is the Faraday's constant, S is the electrode area, Γ_{ET} is the surface concentration of active enzyme, [Fc] is the mediator concentration, [G] is the glucose concentration in the solution. Using the equation and the known rate constant values ($k_2 = 700\ s^{-1}$, $k_3 = 1.2 \times 10^7\ M^{-1}\ s^{-1}$, $k_{red} = 1.1 \times 10^4\ M^{-1}\ s^{-1}$), the surface concentration of GOx immobilized at the enzyme electrode was determined. As shown in Table 1, the total coverage of active glucose oxidase, Γ_{ET}, was linearly proportional to the number of immobilized bilayers, indicating that the multilayer structure involving TFGn and GOx was formed in a spatially ordered manner. It can be seen that the increment of the amount of GOx Γ_E per GOx/TFGn bilayer was 1.52×10^{-12} mol/cm^2, which is 2.5-fold higher than that of the multilayer films containing glucose oxidase reported in another literature [45]. The higher active GOx amount

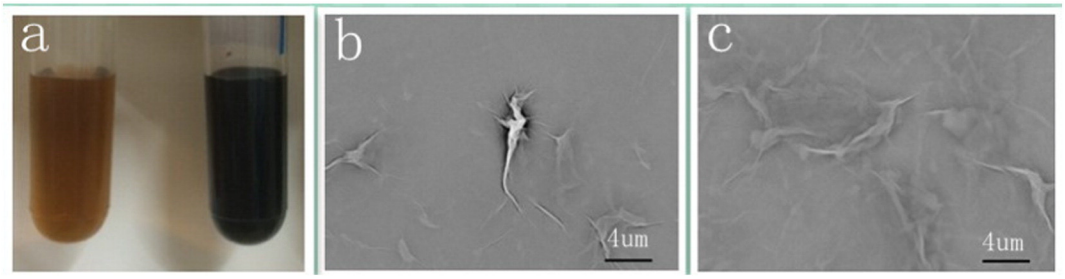

Fig. 4. (a) Photograph of the GO and TFGn dispersed in doubly distilled water. (b) SEM image of GO. (c) SEM image of TFGn.

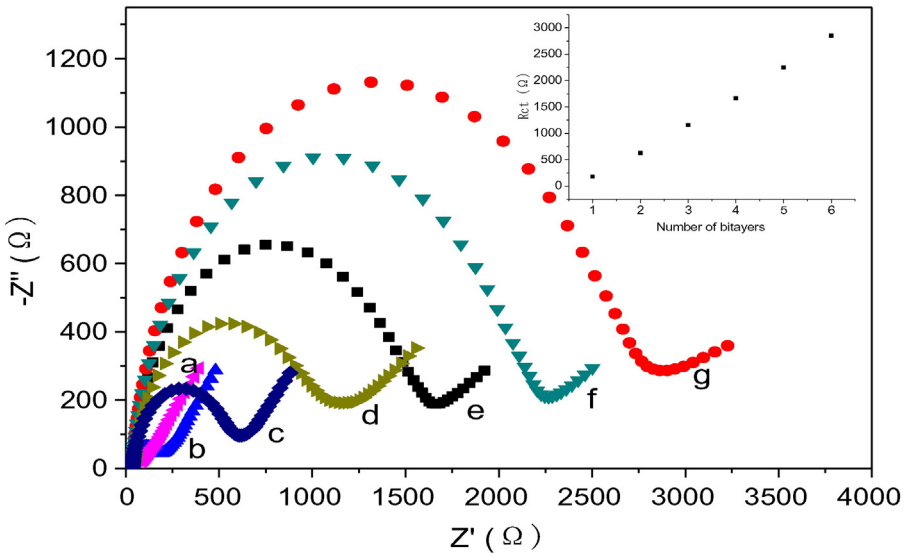

Fig. 5. The electrochemical impedance spectra for the modified gold electrode with different numbers of TFGn/GOx bilayers in 5 mM $K_3[Fe(CN)_6]/K_4[Fe(CN)_6]$ (1:1) solution: (a) bare Au, (b) one bilayer, (c) two bilayers, (d) three bilayers, (e) four bilayers, (f) five bilayers and (g) six bilayers. Inset shows the relationship of Rct vs. the number of bilayers.

on the $Au/CA/(GOx/TFGn)_n$ should be caused by three aspects. First, the TFGn have large specific surface area, which can immobilize more enzyme. Second, the biocompatible TFGn provide a favorable microenvironment, which can retain the bioactivity of glucose oxidase. Third, the layer-by-layer covalent assembly avoids the loss of glucose oxidase.

3.6. Analytical performance of the biosensor

Amperometric analysis was used for the evaluation of the biosensor for glucose detection. Fig. 8(A) shows a current versus time plot for the $Au/CA/(GOx/TFGn)_4$ for successive additions of 1 mM glucose with an applied potential at 0.20 V. As the glucose solution was added to the stirring buffer solution, the biosensor responded rapidly to the substrate. The time required to reach the steady-state current platform was within 6 s, indicating faster charge transport in films with TFGn.

To address the analytical performance of the biosensor, calibration curves were obtained for the $Au/CA/(GOx/TFGn)_n$, where n = 2, 4 and 6 (Fig. 8(B)). The current responses were significantly amplified with an increase in the number of GOx/TFGn bilayers. The sensitivities, calculated from the linear regions of the calibration curves, were 10.25 μA mM^{-1} cm^{-2} for $Au/CA/(GOx/TFGn)_2$, 15.10 μA mM^{-1} cm^{-2} for $Au/CA/(GOx/TFGn)_4$ and 19.9 μA mM^{-1} cm^{-2} for $Au/CA/(GOx/TFGn)_6$. Therefore, the analytical performance of the $Au/CA/(GOx/TFGn)_n$ can be regulated by adjusting the number of GOx/TFGn bilayers. This is significantly different from other graphene-based glucose biosensors, in which glucose oxidase was immobilized in a monolayer of

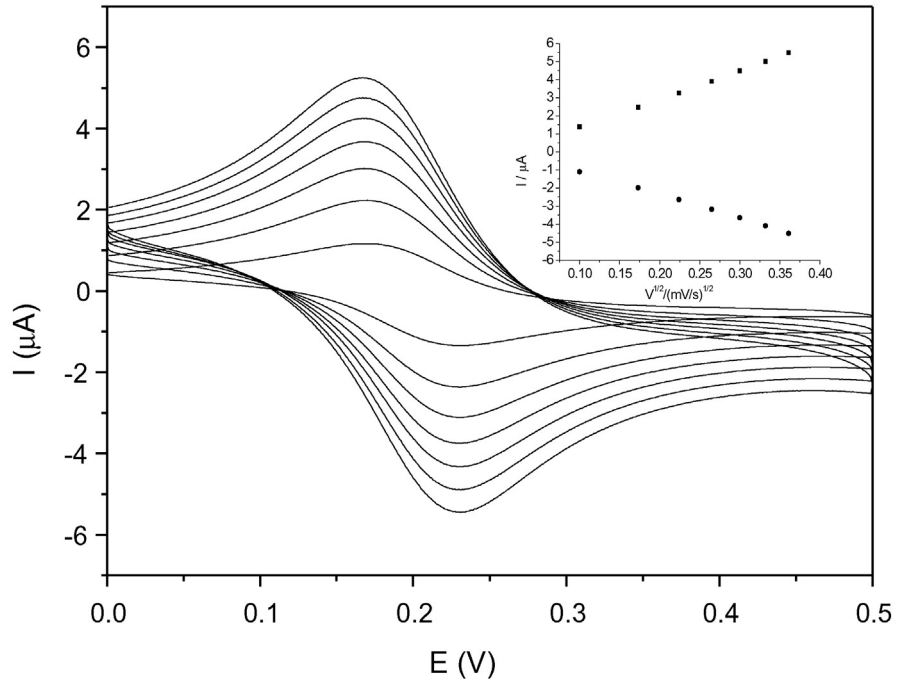

Fig. 6. Cyclic voltammograms of $(GOx/TFGn)_6$ multilayer film electrodes in 0.1 mol/L PBS with a pH 6.8 containing 0.25 mmol/L ferrocenemethanol at the following different scan rates: 10, 30, 50, 70, 90, 110 and 130 mV/s (from inside to outside), respectively. Inset: plot of the anodic and cathodic peak current vs. $V^{1/2}$.

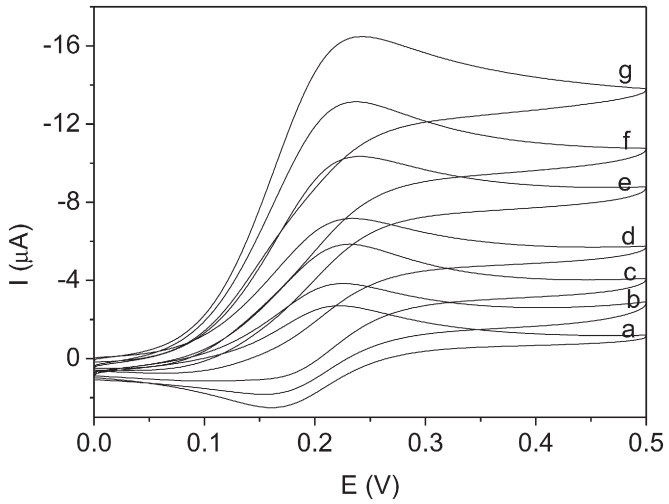

Fig. 7. Cyclic voltammograms of the $(GOx/TFGn)_n$ multilayer electrodes in 0.1 M phosphate buffer solution (pH = 6.8) containing 0.25 mM ferrocenemethanol and 20 mM glucose with the following numbers of bilayers: (a) zero, (b) one, (c) two, (d) three, (e) four, (f) five and (g) six. Scan rate: 50 mV/s.

graphene and thus the amperometric response could not be modulated [7,10,46].

Meanwhile, the layer-by-layer covalent assembly greatly improved the sensitivity of the sensor due to an increase in the fixed glucose oxidase. The sensitivity reached 19.9 μA mM^{-1} cm^{-2} for Au/CA/$(GOx/TFGn)_6$, which is higher than that of the previously reported graphene-based glucose biosensor [20,41,47–49].

3.7. The stability of the sensor

The long-term storage stability of the modified Au/CA/$(GOx/TFGn)_5$ multilayer electrode was evaluated when stored at 4 °C and measured at intervals over five days. About 4% decrease in the catalytic current response to glucose was observed after 2 weeks, and the catalytic current response maintained 90% of its initial value after 30 days, indicating good operational stability. Such excellent stability is attributed to the following aspects: the covalent interaction between TFGn and GOx is strong and not affected by changes such as the temperature, solution pH, and ionic strength. Furthermore, the good biocompatibility of TFGn maintains the biological activity of the enzyme immobilized on the electrode. Finally, the construction process is mild, and no damage is inflicted on the enzyme molecules.

4. Conclusion

The triethylenetetramine-functionalized graphene was successfully prepared from the graphene oxide. FT-IR, XPS and UV spectral characterization corroborated that the triethylenetetramine was grafted onto the GO surface through covalent bonding between amine and epoxy groups, and GO was reduced. XRD and Raman spectra showed that the triethylenetetramine molecules were inserted in the GO sheets to increase the interlayer distances. The resultant TFGn was uniformly dispersed in water and exhibited no aggregation over several weeks, indicating that the introduction of amino groups greatly increased the hydrophilicity of TFGn. Here we applied such TFGn for the construction of glucose biosensors based on layer-by-layer covalent bonding without any cross-linker. The electrodes modified with the $(GOx/TFGn)_n$ multilayer films displayed an outstanding electrocatalytical response to the oxidation of glucose when ferrocenemethanol was used as an artificial redox mediator, and the catalytic response of the resulting Au/CA/$(GOx/TFGn)_n$ electrodes to glucose enhanced significantly with an increasing number of bilayers, revealing that the sensitivity is tunable by controlling the multilayer film thickness.

Table 1
The coverage of active enzyme for different numbers of GOx/TFGn bilayers calculated from the cyclic voltammetric data[a].

Bilayers $(GOx/TFGn)_n$	Γ_{ET} (10^{-12} mol/cm^2)	Γ_E[b] (10^{-12} mol/cm^2)
1	1.30 ± 0.01	–
2	2.82 ± 0.01	1.52
3	4.33 ± 0.01	1.51
4	5.86 ± 0.01	1.53
5	7.38 ± 0.01	1.52
6	8.91 ± 0.01	1.53

[a] Plateau currents were measured by subtracting the glucose-free voltammograms from the mediated (20 mM glucose in solution) voltammograms.
[b] Active enzyme coverage of each layer was calculated from the respective values of Γ_{ET}.

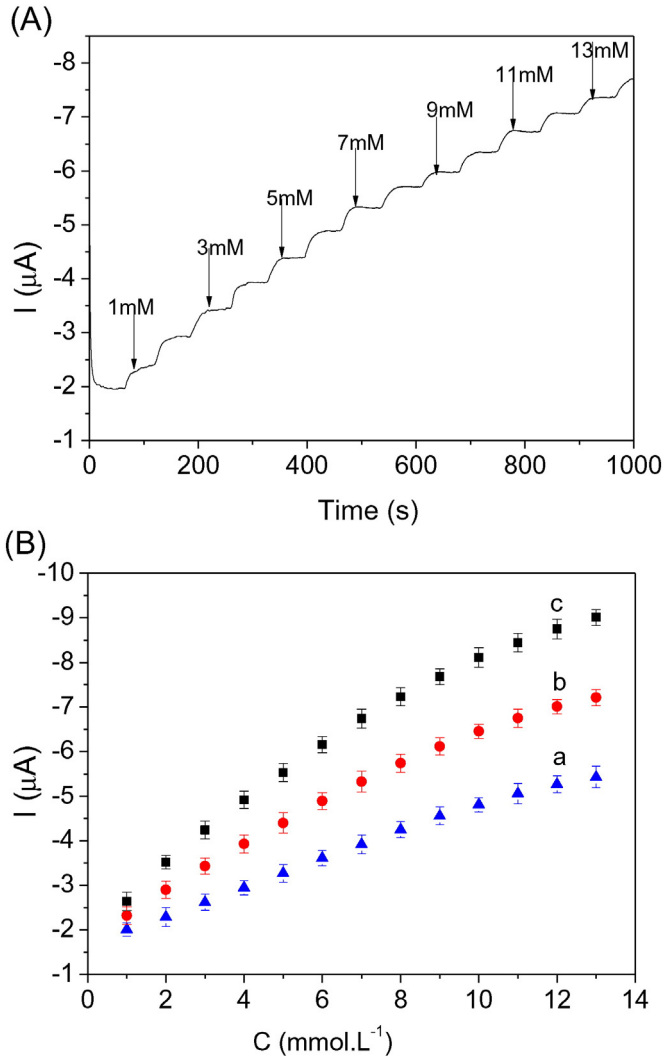

Fig. 8. (A) I versus t curve of the Au/CA/$(GOx/TFGn)_4$ multilayer electrodes upon successive addition of 1 mmol/L glucose to stirred PBS (pH = 6.8) containing 0.25 mM ferrocenemethanol. Applied potential: 0.20 V. (B) Calibrations for the number of $(GOx/TFGn)_n$ bilayers as a function of the glucose concentration: (a) Au/CA/$(GOx/TFGn)_2$, (b) Au/CA/$(GOx/TFGn)_4$ and (c) Au/CA/$(GOx/TFGn)_6$. Bioelectrocatalytic signal values were obtained from the respective current versus time curves. Error bars have been deduced from measurements in triplicate.

Acknowledgements

This work was supported financially by the Science and Technology Program of Shenyang (No. F13-318-1-36), the National Natural Science

Foundation of China (No. 21205081), and the Foundation of Liaoning Educational Committee (No. L2015541).

References

[1] E.C. Sykes, Surface assembly: graphene goes undercover, Nat. Chem. 1 (2009) 175–176.
[2] D. Li, R.B. Kaner, Graphene-based materials, Science 320 (2008) 1170–1171.
[3] H. Liu, S. Ryu, Z. Chen, M.L. Steigerwald, C. Nuckolls, L.E. Brus, Photochemical reactivity of graphene, J. Am. Chem. Soc. 131 (2009) 17099–17101.
[4] R.M. Westervelt, Applied physics. Graphene nanoelectronics, Science 320 (2008) 324–325.
[5] E. Sykes, H. Charles, Editorial comment on: defining early morbidity of radical cystectomy for patients with bladder cancer using a standardized reporting methodology, Nat. Chem. 1 (2009) 175–176.
[6] C. Lee, X. Wei, J.W. Kysar, J. Hone, The antidepressant fluoxetine restores plasticity in the adult visual cortex, Science 321 (2008) 385–388.
[7] L. Hua, X.Q. Wu, R. Wang, Glucose sensor based on an electrochemical reduced graphene oxide-poly(L-lysine) composite film modified GC electrode, Analyst 137 (2012) 5716–5719.
[8] Z. Guo, Z.Y. Wang, H.H. Wang, G.Q. Huang, M.M. Li, Electrochemical sensor for Isoniazid based on the glassy carbon electrode modified with reduced graphene oxide–Au nanomaterials, Mater. Sci. Eng. C 57 (2015) 197–204.
[9] P.H. Deng, Z.F. Xu, Y.L. Feng, Acetylene black paste electrode modified with graphene as the voltammetric sensor for selective determination of tryptophan in the presence of high concentrations of tyrosine, Mater. Sci. Eng. C 35 (2014) 54–60.
[10] D. Zheng, S.K. Vashist, K. Al-Rubeaan, J.H.T. Luong, F.S. Sheu, Mediatorless amperometric glucose biosensing using 3-aminopropyltriethoxysilane-functionalized graphene, Talanta 99 (2012) 22–28.
[11] O. Akhavan, E. Ghaderi, R. Rahighi, Toward single-DNA electrochemical biosensing by graphene nanowalls, ACS Nano 6 (2012) 2904–2916.
[12] O. Akhavana, E. Ghaderi, R. Rahighi, M. Abdolahad, Spongy graphene electrode in electrochemical detection of leukemia at single-cell levels, Carbon 79 (2014) 654–663.
[13] O. Akhavan, E. Ghaderi, E. Hashemi, R. Rahighi, Ultra-sensitive detection of leukemia by graphene, Nanoscale 6 (2014) 14810–14819.
[14] Y. Zhu, A.L. Higginbotham, J.M. Tour, Covalent functionalization of surfactant-wrapped graphene nanoribbons, Chem. Mater. 21 (2009) 5284–5291.
[15] S.H. Ryu, J.H. Sin, A.M. Shanmugharaj, Study on the effect of hexamethylene diamine functionalized graphene oxide on the curing kinetics of epoxy nanocomposites, Eur. Polym. J. 52 (2014) 88–97.
[16] O.C. Compton, D.A. Dikin, K.W. Putz, L.C. Brinson, S.T. Nguyen, Electrically conductive "alkylated" graphene paper via chemical reduction of amine-functionalized graphene oxide paper, Adv. Mater. 22 (2010) 892–896.
[17] S.F. Hou, S.J. Su, M.L. Kasner, P. Shah, K. Patel, C.J. Madarang, Formation of highly stable dispersions of silane-functionalized reduced graphene oxide, Chem. Phys. Lett. 50 (2010) 68–74.
[18] Y. Zhu, J.M. Tour, Graphene nanoribbon thin films using layer-by-layer assembly, Nano Lett. 10 (2010) 4356–4362.
[19] J.Q. Liu, N. Kong, A.H. Li, X. Luo, L. Cui, R. Wang, S.Y. Feng, Graphene bridged enzyme electrodes for glucose biosensing application, Analyst 138 (2013) 2567–2575.
[20] H. Gu, Y.Y. Yu, X.Q. Liu, B. Ni, T.S. Zhou, G.Y. Shi, Layer-by-layer self-assembly of functionalized graphene nanoplates for glucose sensing in vivo integrated with on-line microdialysis system, Biosens. Bioelectron. 32 (2012) 118–126.
[21] J.H. Chen, H.T. Xing, X. Sun, Z.B. Su, Y.H. Huang, W. Wen, S.R. Hu, H.X. Guo, W.B. Wu, Y.S. He, Highly effective removal of Cu(II) by triethylenetetramine-magnetic reduced graphene oxide composite, Appl. Surf. Sci. 356 (2015) 355–363.
[22] J. Jang, V.H. Pham, S.H. Hur, S.C. Jin, J.S. Chung, Dispersibility of reduced alkylamine-functionalized graphene oxides in organic solvents, J. Colloid Interface Sci. 424 (2014) 62–66.
[23] D.C. Marcano, D.V. Kosynkin, J.M. Berlin, A. Sinitskii, Z. Sun, A. Slesarev, L.B. Alemany, W. Lu, J.M. Tour, Improved synthesis of graphene oxide, ACS Nano 4 (2010) 4806–4814.
[24] O.R. Zaborsky, J. Ogletree, The immobilization of glucose oxidase via activation of its carbohydrate residues, Biochem. Biophys. Res. Commun. 61 (1974) 210–216.
[25] J.I. Paredes, S. Villar-Rodil, A. Martínez-Alonso, J.M.D. Tascón, Graphene oxide dispersions in organic solvents, Langmuir 24 (2008) 10560–10564.
[26] S. Rani, M. Kumar, R. Kumar, D. Kumar, S. Sharma, G. Singh, Characterization and dispersibility of improved thermally stable amide functionalized graphene oxide, Mater. Res. Bull. 60 (2014) 143–149.
[27] H.W. Yang, M.Y. Hua, S.L. Che, R.Y. Tsai, Reusable sensor based on high magnetization carboxyl-modified graphene oxide with intrinsic hydrogen peroxide catalytic activity for hydrogen peroxide and glucose detection, Biosens. Bioelectron. 41 (2013) 172–179.
[28] J. Tian, P.X. Yuan, D. Shan, S.N. Ding, G.Y. Zhang, X.J. Zhang, Biosensing platform based on graphene oxide via self-assembly induced by synergic interactions, Anal. Biochem. 460 (2014) 16–21.
[29] S.H. Ryu, J.H. Sin, A.M. Shanmugharaj, Influence of hexamethylene diamine functionalized graphene oxide on the melt crystallization and properties of polypropylene nanocomposites, Mater. Chem. Phys. 146 (2014) 478–486.
[30] O. Akhavan, E. Ghaderi, S. Aghayee, Y. Fereydooni, A. Talebi, The use of a glucose-reduced graphene oxide suspension for photothermal cancer therapy, J. Mater. Chem. 22 (2012) 13773–13781.
[31] A. Esfandiar, O. Akhavan, A. Irajizad, Melatonin as a powerful bio-antioxidant for reduction of graphene oxide, J. Mater. Chem. 21 (2011) 10907–10914.
[32] D. Yang, A. Velamakanni, G. Bozoklu, S. Park, M. Stoller, R.D. Piner, S. Stankovich, I. Jung, D.A. Field, C.A. Ventrice Jr., R.S. Ruoff, Chemical analysis of graphene oxide films after heat and chemical treatments by X-ray photoelectron and micro-Raman spectroscopy, Carbon 47 (2009) 145–152.
[33] Z.J. Fan, W. Kai, J. Yan, T. Wei, L.J. Zhi, J. Feng, Y.M. Ren, L.P. Song, F. Wei, Facile synthesis of graphene nanosheets via Fe reduction of exfoliated graphite oxide, ACS Nano 5 (2011) 191–198.
[34] A.C. Ferrari, J.C. Meyer, V. Scardaci, C. Casiraghi, M. Lazzeri, F. Mauri, S. Piscanec, D. Jiang, K.S. Novoselov, S. Roth, A.K. Geim, Raman spectrum of graphene and graphene layers, Phys. Rev. Lett. 97 (2006) 187401–187404.
[35] I. Calizo, A.A. Balandin, W. Bao, F. Miao, C.N. Lau, Temperature dependence of the Raman spectra of graphene and graphene multilayers, Nano Lett. 7 (2007) 2645–2649.
[36] K.S. Kim, Y. Zhao, H. Jang, S.Y. Lee, J.M. Kim, K.S. Kim, J.H. Ahn, P. Kim, J.Y. Choi, B.H. Hong, Large-scale pattern growth of graphene films for stretchable transparent electrodes, Nature 457 (2009) 706–710.
[37] K.N. Kudin, B. Ozbas, H.C. Schniepp, R.K. Prud'Homme, I.A. Aksay, R. Car, Raman spectra of graphite oxide and functionalized graphene sheets, Nano Lett. 8 (2008) 36–41.
[38] O. Akhavan, Bacteriorhodopsin as a superior substitute for hydrazine in chemical reduction of single-layer graphene oxide sheets, Carbon 81 (2015) 158–166.
[39] C.S. Shan, H.F. Yang, J.F. Song, D.X. Han, A. Ivaska, L. Niu, Direct electrochemistry of glucose oxidase and biosensing for glucose based on graphene, Anal. Chem. 81 (2009) 2378–2382.
[40] R.S. Dey, C.R. Raj, Redox-functionalized graphene oxide architecture for the development of amperometric biosensing platform, ACS Appl. Mater. Interfaces 5 (2013) 4791–4798.
[41] G.H. Zeng, Y.B. Xing, J. Gao, Z.Q. Wang, X. Zhang, Unconventional layer-by-layer assembly of graphene multilayer films for enzyme-based glucose and maltose biosensing, Langmuir 26 (2010) 15022–15026.
[42] R. Ehret, W. Baumann, M. Brischwein, A. Schwinde, K. Stegbauer, B. Wolf, Monitoring of cellular behaviour by impedance measurements on interdigitated electrode structures, Biosens. Bioelectron. 12 (1997) 29–41.
[43] C. Bourdillon, C. Demaille, J. Gueris, J. Moiroux, J.-M. Savéant, A fully active monolayer enzyme electrode derivatized by antigen-antibody attachment, J. Am. Chem. Soc. 115 (1993) 12264–12269.
[44] N. Anicet, C. Bourdillon, J. Moiroux, J.-M. Savéant, Electron transfer in organized assemblies of biomolecules. Step-by-step avidin/biotin construction and dynamic characteristics of a spatially ordered multilayer enzyme electrode, J. Phys. Chem. B 102 (1998) 9844–9849.
[45] Y.Y. Sun, F. Yan, W.S. Yang, C.Q. Sun, Multilayered construction of glucose oxidase and silica nanoparticles on Au electrodes based on layer-by-layer covalent attachment, Biomaterials 27 (2006) 4042–4049.
[46] F.Y. Kong, S.X. Gu, W.W. Li, T.T. Chen, Q. Xu, W. Wang, A paper disk equipped with graphene/polyaniline/Au nanoparticles/glucose oxidase biocomposite modified screen-printed electrode: toward whole blood glucose determination, Biosens. Bioelectron. 56 (2014) 77–82.
[47] M. Veerapandian, Y.T. Seo, H. Shin, K. Yun, M.H. Lee, Functionalized graphene oxide for clinical glucose biosensing in urine and serum samples, Int. J. Nanomedicine 7 (2012) 6123–6136.
[48] H.D. Jang, S.K. Kim, H. Chang, K.M. Roh, J.W. Choi, J. Huang, A glucose biosensor based on TiO_2–graphene composite, Biosens. Bioelectron. 38 (2012) 184–188.
[49] C.S. Shan, H.F. Yang, D.X. Han, Q.X. Zhang, A. Ivaska, L. Niu, Graphene/AuNPs/chitosan nanocomposites film for glucose biosensing, Biosens. Bioelectron. 25 (2010) 1070–1074.